

SL-SLAM: A robust visual-inertial SLAM based deep feature extraction and matching

Xiao Zhang, Shuaixin Li

Abstract—This paper explores how deep learning techniques can improve visual-based SLAM performance in challenging environments. By combining deep feature extraction and deep matching methods, we introduce a versatile hybrid visual SLAM system designed to enhance adaptability in challenging scenarios, such as low-light conditions, dynamic lighting, weak-texture areas, and severe jitter. Our system supports multiple modes, including monocular, stereo, monocular-inertial, and stereo-inertial configurations. We also perform analysis how to combine visual SLAM with deep learning methods to enlighten other researches. Through extensive experiments on both public datasets and self-sampled data, we demonstrate the superiority of the SL-SLAM system over traditional approaches. The experimental results show that SL-SLAM outperforms state-of-the-art SLAM algorithms in terms of localization accuracy and tracking robustness. For the benefit of community, we make public the source code at <https://github.com/zzzxxxx111/SLslam>.

Index Terms—Hybrid SLAM, deep learning, deep feature, feature matching, inertial navigation, robustness, complex environments.

I. INTRODUCTION

SLAM (Simultaneous Localization and Mapping) is a pivotal technology within robotics [1], autonomous driving [2], and 3D reconstruction [3], where it simultaneously determines the sensor position (localization) while building a map of the environment [4]. Vision and inertial sensors are the most commonly used sensing devices, and related solutions have been deeply discussed and explored. After decades of development, the processing architecture of visual (inertial) SLAM has a basic framework, including Tracking, Mapping, Loop closure. In recent years, related research has focused on improving robustness and adaptability under extreme conditions.

Due to the long history of the development of SLAM technology, there are many representative works of SLAM based on traditional geometric methods, such as ORBSLAM [5], VINS-Mono [6], DVO [7], MSCKF [8]. However, there are still some unresolved issues. In challenging environments such as low or dynamic lighting, severe jitter, and areas with weak textures, Due to the fact that traditional feature extraction algorithms only consider local information in images and do not take into account the structure and semantic information of images, when encountering the aforementioned situations, Existing SLAM systems may struggle due to difficulty of extracting and matching accurate and stable features. Consequently, the tracking of SLAM systems may become unstable or even ineffective under these conditions.

The rapid advancement of deep learning has ushered in revolutionary changes in the realm of computer vision. By leveraging extensive data training, deep learning models can assimilate intricate scene structures and semantic information, thereby enhancing SLAM system's understanding and expression ability of the scene. This approach is mainly divided into two routes. The first involves end-to-end algorithms based on deep learning, such as Droid-slam [9], NICE-SLAM [10], DVI-SLAM [11]. However, these methods require a large amount of data for training, as well as high computational resources and storage space, and struggle to achieve real-time tracking. Furthermore, they may excel only in specific scenarios that have similar training datasets. When facing the complex environment, its estimated trajectories tend to be offset or even invalid. The second route named hybrid SLAM utilizes deep learning to enhance specific modules within SLAM. Hybrid SLAM makes full use of the advantages of traditional geometric methods and deep learning methods. It can strike a balance between geometric constraints and semantic understanding. Although there is some research in this area currently, how to effectively integrate deep learning techniques remains a worthwhile direction for further study. At present, the existing hybrid slam has some limitations, DX-Net [12] simply replace ORB feature points with deep feature points, but continues to utilize traditional methods for tracking these features. Therefore, this may lead to the incoherence of the deep feature information. SP-Loop [13] introduce deep learning feature points solely into the closed-loop module, retaining traditional feature point extraction methods elsewhere. Therefore, these hybrid SLAM methods do not effectively and comprehensively combine deep learning technology, which leads to the degradation of tracking and mapping effects in some complex scenes.

To address these problem, we propose a deep learning-based versatile SLAM system. We incorporate the Superpoint feature point extraction module into the system, and this feature is used as the sole representation throughout. Additionally, in complex environments, traditional feature matching methods often exhibit instability, leading to a degradation in tracking and mapping quality. However, recent advancements in feature matching methods based on deep learning have shown promise in achieving improved matching performance in such complex environments. These methods leverage prior information and structural details of scenes to enhance matching effectiveness. Lightglue [14], as the most recent SOTA matching method, proves advantageous for SLAM systems requiring high real-time performance due to its efficiency and lightweight nature. Consequently, we've replaced the feature matching method

This paper was produced by the IEEE Publication Technology Group. They are in Piscataway, NJ.

Manuscript received April 19, 2021; revised August 16, 2021.

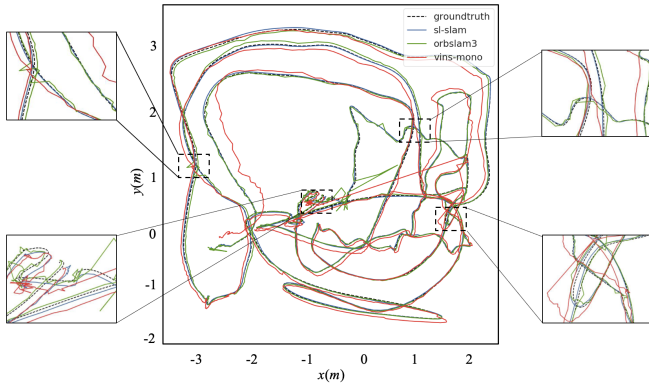


Fig. 1. Trajectory comparison between ORB-SLAM3, vins-mono and sl-slam. In the Euroc's difficult sequence V203.

across the entire SLAM system with Lightglue, enhancing robustness and accuracy over traditional methods. Furthermore, we've preprocessed the Superpoint feature point descriptor to align with the training of the corresponding visual word bag. When combined with Lightglue, this approach achieves precise scene recognition effect. Simultaneously, to maintain a balance between accuracy and efficiency, we design a feature point selection strategy. Taking into account scalability, portability, and real-time performance, we leverage the ONNX Runtime library to deploy these deep learning models. Finally, we design a series of experiments to prove that our method improves the trajectory prediction accuracy of SLAM algorithm and the tracking robustness in a variety of challenging scenarios, as show in Fig.8. In summary, our contributions in this work encompass the following key points:

- 1) We developed the first versatile simultaneous localization and photorealistic mapping system based deep feature extraction and matching. The framework supports monocular, stereo, monocular-inertial, stereo-inertial sensor in various environments.
- 2) To better adapt to challenging environment, we apply deep feature extraction and matching to the whole process of SLAM system, including tracking, local mapping, and loop closure. Adaptive feature screening as well as deep feature bag of words adaptation to SLAM system are designed.
- 3) We conduct extensive experiments to demonstrate the effectiveness and robustness, and the results on public datasets and self-collected datasets show that our system is superior to other start-of-the-art SLAM systems. The system is fully implemented in C++ and ONNX, and it can run at real-time speed. We release the source code at <https://github.com/zzzzxxxx111/SLslam> to benefit the community.

II. RELATED WORK

A. Traditional visual SLAM works

The development history of SLAM, rooted in traditional geometric method, has yielded numerous classic and successful approaches. According to their differing approaches to feature

representation, these algorithms can be broadly categorized into feature point SLAM and direct SLAM.

Feature-point SLAM relies on a limited number of distinct feature points for matching and tracking. It excels in environments with prominent features and is well suited for applications with stringent real-time requirements. Notable among these algorithms is ORB-SLAM3 [15], which utilizes ORB feature points to describe scenes. It employs three parallel threads for tracking, local mapping, and loop closure, allowing trajectory estimation and optimization. Another leading algorithm in this category is Vins-mono [6], which is a tightly coupled visual-inertial slam system, and employs a good feature-to-track algorithm for feature point extraction and tracking. Additionally, OpenVSLAM [16] stands out for its versatility in handling various camera models, facilitating map creation, storage, and positioning operations based on pre-existing maps. DSO [17] stands out as a representative work in direct SLAM, based on the photometric invariance assumption. This is achieved by sampling pixels with intensity gradients in the image and integrating the photometric error model and all model parameters into the optimization function for joint optimization. However, it requires more information from the pixels, which leads to a high computational complexity.

One common issue with SLAM based on traditional image processing methods is the inability to perceive geometric and structural information in the scene. This limitation becomes evident in environments with weak or flickering light, or significant camera shake, where accurate camera pose estimation becomes challenging, sometimes resulting in lost tracking. To address these challenges, many researchers are integrating deep learning into SLAM systems to enhance robustness.

B. Deep learning-based visual SLAM works

Visual SLAM frameworks based on deep learning can be broadly categorized into two groups: end-to-end frameworks and hybrid SLAM frameworks. UnDeepVO [18] stands out as the first end-to-end visual odometry framework based on neural networks. It leverages binocular image training to recover absolute scale by utilizing spatial and temporal geometric constraints. However, compared to traditional SLAM algorithms, UnDeepVO may lack in accuracy and robustness. D3VO [19] addresses the challenge of image depth estimation in occluded and dynamic environments by incorporating a Bayesian filtering method. This approach quantifies uncertainty for each pixel, leading to improved accuracy and performance in pose estimation. DROID-SLAM [9] introduces a microloop optimization heuristic design, enhancing the network's performance and generalization capabilities. DPVO [20] utilizes a feature-based patch representation to encode local scene information. It employs a novel recurrent network structure to incorporate temporal information for tracking these image patches. While end-to-end algorithms like these offer versatility across various application scenarios, they typically require extensive datasets and computing resources for training. In addition, they may experience performance degradation when transitioning to different scenarios.

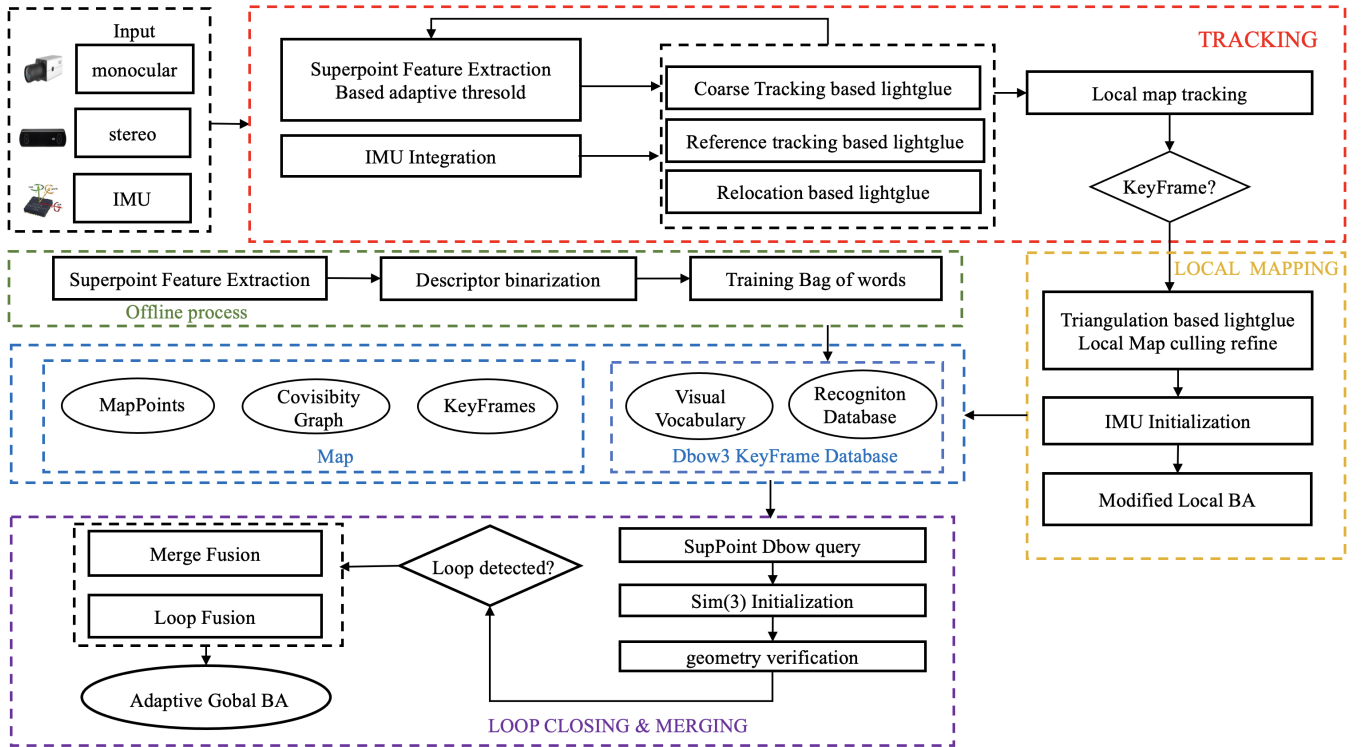


Fig. 2. The framework of SL-SLAM.

different schemes of integrating deep learning methods: feature extraction, optical flow, map, end-to-end, etc. Hybrid SLAM frameworks maintain the modular structure of traditional SLAM frameworks while integrating deep learning modules to enhance overall system performance. These frameworks often replace or augment traditional components with deep learning techniques. Lift-SLAM [21] utilizes the Learned Invariant Feature Transform (LIFT) network to extract features within the backend of a traditional ORB-SLAM system. Similarly, GCNv2SLAM [22] employs a Geometric Correspondence Network (GCN) to extract feature points and descriptors of the scene. DX-SLAM [12] adapts ORB features in ORB-SLAM2 to superpoint features and uses the OpenVINO toolkit for model deployment. However, these approaches still rely on traditional methods for feature extraction and matching during tracking, which can lead to poor tracking performance in challenging environments. AirVO [23] stands out by using superpoint feature points and superglue for feature matching. It utilizes point- and line-feature reprojection errors to jointly optimize the pose, improving robustness in complex environments. However, it's worth noting that AirVO is not a complete SLAM system and can only accept RGB-D input.

III. METHOD

A. The System Overview

The SL-SLAM's system structure is shown in Fig. 2, This system primarily has four sensor configurations, namely monocular, monocular-inertial, stereo, and stereo-inertial.

Building upon ORB-SLAM3 as the baseline, the system comprises three primary modules: Tracking, Local Mapping, and Loop Closure. To integrate deep learning models into the system, the ONNX Runtime deep learning deployment framework is used, incorporating the superpoint and lightglue models.

For each incoming image, the system first feeds it into the SuperPoint network to obtain probability tensors for feature points and descriptor tensors. The system then uses two frames for initialization and performs coarse tracking on each subsequent frame. It further refines the pose estimation by tracking the local map. In the event of tracking failure, the system utilizes either tracking with a reference frame or performs relocalization to obtain the pose again. Note that lightglue is used for feature matching in coarse tracking, initialization, reference frame tracking, and relocalization. This ensures accurate and robust matching relationships, thereby enhancing the effectiveness of tracking.

In the baseline algorithm, the main role of the local mapping thread is to dynamically construct a local map in real-time, which includes map points and keyframes. It utilizes the local map to perform bundle adjustment optimization, thereby reducing tracking errors and enhancing consistency. The local mapping thread reconstructs precise map points using keyframes output by the tracking thread, employing LightGlue-based triangulation and adaptive local Bundle Adjustment (BA) optimization. Redundant map points and keyframes are then distinguished and removed.

The closed-loop correction thread utilizes the keyframe database and bag-of-words trained on superpoint descriptors

to retrieve similar keyframes. Binarization of superpoint descriptors is employed to enhance retrieval efficacy. Selected key frames undergo feature matching using lightglue for common-view geometric verification, reducing the likelihood of mismatches. Finally, closed-loop fusion and global BA are executed to optimize the overall pose. Further details are elaborated in subsequent sections.

B. Feature Extraction

1) *Superpoint Network structure*: The SuperPoint network architecture consists primarily of three components: a shared encoder, a feature detection decoder, and a descriptor decoder. The encoder is a VGG-style network that can decrease the image dimension and extract features. The feature detection decoder is tasked with computing the probability for each pixel of the image to determine its likelihood of being a feature point. The descriptor decoding network utilizes the sub-pixel convolution to mitigate the computational complexity of the decoding process. The network then outputs a semi-dense descriptor, followed by applying the bicubic interpolation algorithm to acquire the complete descriptor. After obtaining the feature point tensor and descriptor tensor of the network output, in order to improve the robustness of feature extraction, we use an adaptive threshold selection strategy to filter out feature points and perform post-processing operations to obtain the feature points and its descriptors. The specific structure of the feature extraction module is shown in Fig.3

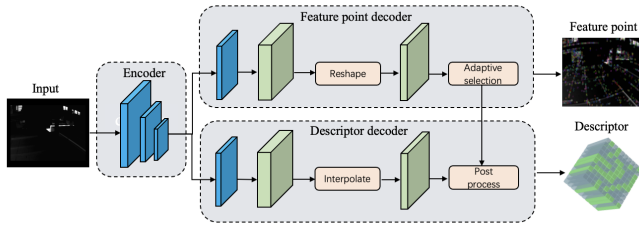


Fig. 3. Overview of feature extraction

2) *Adaptive feature selection*: Initially, each image, denoted as $I(W \times H)$, undergoes a conversion to grayscale before being resized to match the dimensions of the input image of the SuperPoint network ($W' \times H'$). An image that's too small might hinder feature extraction, thus deteriorating tracking performance, while overly large images could lead to excessive computational demands and memory usage. Therefore, in order to balance the feature extraction accuracy and efficiency, the paper selects $W' = 400$ and $H' = 300$. Consequently, a tensor of size $W' \times H'$ is fed into the network, producing two output tensors: the score tensor S in $R^{H' \times W'}$ and the descriptor tensor D in $R^{1 \times L \times \frac{W'}{8} \times \frac{H'}{8}}$.

Once the feature point score tensor and the feature descriptor are obtained, the next step involves setting a threshold th to filter the feature points, as shown in equation 1:

$$S' = \begin{cases} S'_{i,j} | S'_{i,j} = \begin{cases} S_{i,j} & \text{if } (i,j) > th \\ 0 & \text{else} \end{cases} \end{cases} \quad (1)$$

In challenging scenes, the confidence of each feature point diminishes, which can lead to fewer features being extracted if a fixed confidence threshold th is employed. To address this issue, we introduce a self-adjusting SuperPoint threshold setting strategy. This adaptive approach dynamically tunes the threshold for feature extraction based on the scene, thereby enabling more robust feature extraction in challenging scenarios. The adaptive threshold mechanism considers two factors: intra-feature relationship and inter-frame feature relationship.

The intra-feature relationship refers to the distribution of feature points across all positions in the frame. Initially, we need to calculate the expectation E and variance σ^2 of the confidence distribution of the feature points within each frame. If we assume that the confidence distribution of feature points follows a Gaussian distribution, the number of feature points within the range $[E + \frac{\sqrt{\sigma^2}}{2}, +\infty)$ should remain constant, ensuring consistent feature extraction and avoiding situations where fixed thresholds may fail to extract sufficient feature points. The inter-frame feature relationship assesses the match quality between the current frame and adjacent frames. Since the interval of each frame is close, the matching quality of the previous frame can roughly reflect the matching quality of this frame. Let m denote the number of feature points matched between the current and adjacent frames. A decrease in matches signals a weak texture area or significant motion, indicating the need for extracting more feature points for subsequent tracking. Conversely, a strong match suggests a rich texture area, allowing for reduced feature extraction and lower computational costs. The adaptive threshold calculation formula is given in eq.2, where μ_1, μ_2 are hyperparameters.

$$th = E + \frac{\sqrt{\sigma^2}}{2} + \mu_1 \frac{1}{(1 + \exp(-\mu_2 m))} \quad (2)$$

Following the adaptive thresholding process, we select the positions $\{(i'_k, v'_k)\}_{k=1}^m$ of m feature points. Subsequently, the descriptor $\{f_k\}_{k=1}^m$ at each position is obtained by utilizing the descriptor tensor. The feature point $\{f_k\}_{k=1}^m$ will be transformed to the size of the original image using the eq.3:

$$f_k = \left(\frac{u'_k \cdot H}{H'}, \frac{v'_k \cdot W}{W'} \right) \quad (3)$$

C. Feature Matching and Front-end

1) *Lightglue network structure*: The LightGlue model comprises multiple identical layers processing two feature sets collectively. Each layer contains self-attention and cross-attention units to update point representations. A classifier in each layer determines inference halting, avoiding unnecessary computations. Finally, a lightweight head computes partial matches scores. The network depth dynamically adjusts based on input image complexity. If image pairs are easily matched, early termination is possible due to high token confidence. Therefore, LightGlue has shorter runtime and lower memory consumption, making it suitable for integration into tasks that require real-time performance.

Given two sets of feature points extracted from images A and B, where image A has M feature points and image B has N feature points, we denote the feature points of image A as

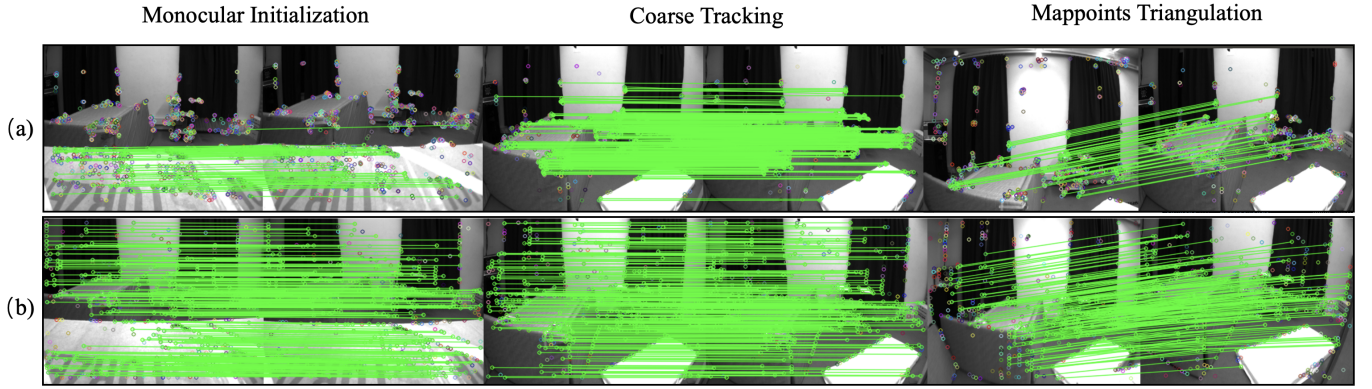


Fig. 4. Comparison of Matching Performance with Different Feature Matching Methods. figure 4(a) and figure 4(b) show the matching effect of orbslam3 and sl-slam algorithms respectively

$\mathcal{A} = \{f_k^A\}_{k=1}^M$ and those of image B as $\mathcal{B} = \{f_k^B\}_{k=1}^N$. We need to normalize each feature point f_k to fall within the range of 0 to 1. The description of the feature points is represented as $d_k \in \mathbb{R}^d$. After feeding them into the Lightglue’s network, The soft partial assignment matrix $P \in [0, 1]^{M \times N}$ will be output. it’s element p_{ij} denotes the likelihood that the i th feature point of image A matches the j th feature point of image B.

2) *Tracking combined with Lightglue*: Due to the short time interval between adjacent frames, typically just tens of milliseconds, ORB-SLAM3 assumes that the camera undergoes uniform motion during this brief period. It estimates the current frame’s pose using the pose and velocity from the previous frame and performs projection matching using this estimated pose. It then searches for matching points within a certain range and refines the pose accordingly. However, in reality, the camera’s motion may not always be uniform. Sudden acceleration, deceleration, or rotation can adversely affect the effectiveness of this approach. Lightglue can effectively address this issue by directly matching features between the current frame and the previous one. It then uses these matched features to refine the initial pose estimation, thereby reducing the negative impact of sudden accelerations or rotations.

In cases where image tracking fails in previous frames, either due to sudden camera movements or other factors, it is necessary to track or relocalize using reference keyframes. The baseline algorithm employs a Bag-of-Words (BoW) approach to accelerate feature matching between the current frame and reference frames. However, the BoW approach converts spatial information into statistical information based on visual vocabulary, potentially losing the accurate spatial relationships between feature points. Additionally, if the visual vocabulary used in the BoW model is insufficient or not representative enough, it may fail to capture the rich features of the scene, leading to inaccuracies in the matching process.

To address these issues, we have replaced the BoW approach with lightglue throughout our system. This change has significantly improved the probability of successful tracking and relocalization under large-scale transformations, thereby enhancing the accuracy and robustness of our tracking process. The effectiveness of different matching methods is shown

in the Fig.4. It can be observed that the matching method based on lightglue demonstrates superior matching performance compared to the projection-based or bag-of-words matching methods employed in ORB-SLAM3. Consequently, during the SLAM operation, it enables the tracking of map points that are more evenly distributed and stable, as illustrated in Fig.6.

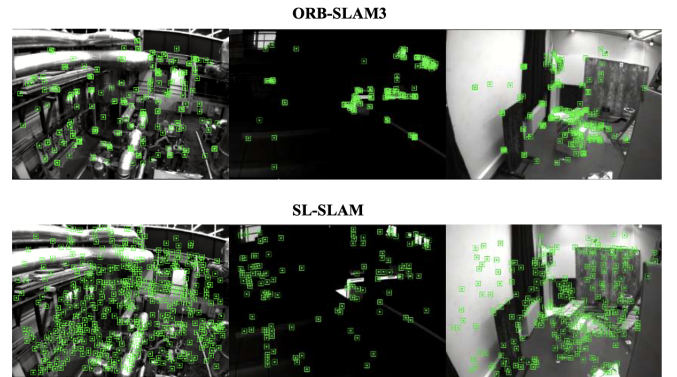


Fig. 5. Tracking Map Points Comparison between SL-SLAM and ORB-SLAM3

3) *local mapping combined with lightglue*: In the local mapping thread, triangulation of new map points is performed using the current keyframe and its neighboring keyframes. To obtain more accurate map points, it is necessary to match with keyframes that have a larger baseline. However, ORB-SLAM3 uses Bag-of-Words (BoW) matching for this purpose, and the performance of BoW feature matching decreases when the baseline is large. In contrast, the lightglue algorithm is well-suited for matching with large baselines and can seamlessly integrate into the system. By utilizing lightglue for feature matching and triangulating the matched points, more comprehensive and higher-quality map points can be recovered. This enhances the local mapping capability by establishing more connections between keyframes and stabilizing tracking through collaborative optimization of the poses of co-visible keyframes and map points. The effect of triangulating map points is shown in Fig.6. It can be observed that, compared to ORB-SLAM3, the map points constructed by our method

can better reflect the structural information of the scene. Additionally, they are distributed more evenly and extensively.

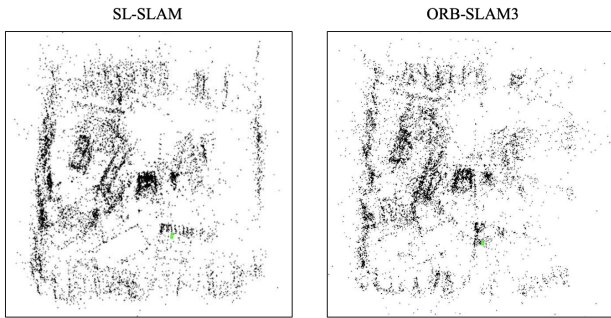


Fig. 6. Map Points Reconstruction Comparison between SL-SLAM and ORB-SLAM3

D. Loop closure

1) *Bag of word deep descriptor*: The bag-of-words approach used in loop closure detection is a visual vocabulary-based method, borrowing the concept from bag-of-words in natural language processing. It begins with offline training of the dictionary. Initially, feature descriptors detected in the training image set are clustered into k sets using K-means, forming the first level of the dictionary tree. Subsequently, recursive operations are performed within each set, resulting in the final dictionary tree with depth L and branch number k , establishing the visual vocabulary. Each leaf node is considered a word.

Once the dictionary is trained, during algorithm execution, online generation of bag-of-words vectors and feature vectors is conducted from all feature points of the current image. The mainstream SLAM frameworks prefer using manually set binary descriptors due to their small memory footprint and simple comparison method. To further enhance method efficiency, SP-Loop [24] represents the value of the superpoint descriptor using a Gaussian distribution with an expected value dimension of 0 and a standard deviation of 0.07. Consequently, the 256-dimensional floating-point descriptor of superpoint can be binary encoded to improve the query speed of visual place recognition. The binary encoding is given in the eq.4.

$$v_i = \begin{cases} 1, & \text{if } v_i \geq 0 \\ 0, & \text{otherwise} \end{cases} \quad (4)$$

2) *fundamental procedure*: Loop closure detection in SLAM (Simultaneous Localization and Mapping) typically involves three key stages: seeking initial loop closure candidate keyframes, verifying loop closure candidate keyframes, and performing loop closure correction alongside global Bundle Adjustment (BA).

To initiate the process, the first step is to identify initial loop closure candidates. This is achieved by leveraging the DBoW3 bag-of-words model trained previously. Keyframes containing common words with the current frame K_a are identified, excluding keyframes covisible K_a . The collective

score of the co-visible keyframes associated with these candidate keyframes is computed. From the top N groups with the highest scores among the closed-loop candidate keyframes, the keyframe with the highest score is selected. This selected keyframe, denoted as K_m .

It is necessary to determinate the relative pose transformation T_{am} from K_m to the current keyframe K_a . In ORB-SLAM3, the feature matching method based bag-of-words is employed to match the current keyframe with the candidate keyframe K_m and its co-visible keyframe K_{co} . It is worth noting that matching the current frame with the candidate frame K_m yields high-quality map point correspondences, since the matching efficiency is significantly enhanced by the lightglue algorithm. Subsequently, the RANSAC algorithm is applied to eliminate outliers, and the Sim(3) transformation is solved to ascertain the initial relative pose T_{am} . In order to avoid wrong location recognition, the candidate keyframes will be geometically verified, the subsequent steps is similar to ORB-SLAM3.

IV. EXPERIMENT

A. Implementation Details

In this section, we provide a detailed description of the parameter settings, experimental procedures, evaluation methods, and characteristics of both publicly available datasets and self-collected datasets for SL-SLAM. The SL-SLAM algorithm is validated on these datasets through qualitative and quantitative analyses, demonstrating its effectiveness. All experiments are conducted on a computer equipped with an Intel Core i7-11700 CPU, 32GB of RAM, and an NVIDIA RTX 3080 GPU, and it runs on Ubuntu18.04 operating system.

In our experiments, we employ the Root Mean Square Error (RMSE) of the Absolute Trajectory Error (ATE) to evaluate the accuracy of pose estimation. ATE is a metric used to assess the disparity between the camera pose trajectories output by the SLAM system and the ground truth camera pose trajectories. RMSE quantifies these errors by computing the square root of the average sum of squared errors over all frames. A smaller RMSE indicates better consistency between the SLAM system's output trajectory and the ground truth trajectory.

We tested our proposed method on three datasets: Euroc [25], TUM-VI [26], and own dataset collected from real-world environments with various challenging conditions. To ensure the flexibility, scalability, and real-time performance of our algorithm, we deployed the deep learning models using the ONNX Runtime deployment framework. Experimental results show that our method can achieve real-time running speed with low GPU memory usage.

The formula for ATE (Absolute Trajectory Error) is shown in Eq.5:

$$RMSE_{ATE} = \sqrt{\frac{1}{N} \sum_{i=1}^N \|T_{gt}^i - T_{est}^i\|_2^2} \quad (5)$$

Where N is the total number of frames in the trajectory. T_{est}^i is the position vector of the estimated trajectory at the i -th frame. T_{gt}^i is the position vector of the ground truth trajectory at the i -th frame. $\|\cdot\|$ represents the Euclidean distance.

TABLE I
RMSE[M] OF ATE COMPARISON WITH STATE-OF-THE-ART VINS METHODS ON EUROC. × MEANS IT FAILS IN THIS SEQUENCE.
THE BEST RESULT IS HIGHLIGHTED IN BOLD.

Dataset	VI-DSO	VI-ORB	OKVIS	VINS-Mono	ORB-SLAM3	DVI-SLAM	SP-Loop	IMPS	Ours
V1_01	0.109	0.095	0.090	0.146	0.091	0.074	0.042	0.090	0.034
V1_02	0.067	0.063	0.122	0.311	0.063	0.114	0.034	0.061	0.019
V1_03	0.096	×	0.196	0.329	0.066	0.083	0.082	0.061	0.031
V2_01	0.075	0.081	0.168	0.124	0.076	0.091	0.038	0.074	0.024
V2_02	0.062	0.080	0.182	0.277	0.058	0.045	0.054	0.056	0.018
V2_03	0.204	0.114	0.305	0.323	0.063	0.072	0.100	0.065	0.024
MH_01	0.074	0.105	0.292	0.177	0.044	0.063	0.070	0.039	0.048
MH_02	0.044	0.067	0.361	0.183	0.083	0.066	0.044	0.058	0.049
MH_03	0.124	0.040	0.267	0.404	0.044	0.101	0.068	0.040	0.039
MH_04	0.112	0.075	0.366	0.394	0.082	0.187	0.100	0.054	0.052
MH_05	0.121	0.152	0.396	0.382	0.064	0.163	0.09	0.058	0.048

B. Accuracy Comparison

In the localization accuracy evaluation of SL-SLAM, the Euroc dataset was selected. The recording scenes in the Euroc dataset include office and factory environments, among others, with three difficulty levels: easy (MH01/2, V101, V201), medium (MH03/4, V102, V202), and difficult (MH05, V103, V203). The difficult level includes variable lighting conditions, severe shaking, and dark environments, providing diverse scenarios and challenges.

In the experiments, we selected several state-of-the-art SLAM algorithms for comparison, including traditional visual-inertial SLAM methods like VI-DSO [27], VI-ORB [28], OKVIS [29], VINS-Mono [6], ORB-SLAM3 [15], and hybrid SLAM algorithm with open-source code such as SP-Loop [24]. and the SOTA end-to-end deep learning SLAM algorithm DVI-SLAM [30]. We compared the trajectories in the Euroc dataset from both quantitative and qualitative perspectives. Quantitative results of the experiments are presented in Table I. SL-SLAM also exhibited significant advantages over other algorithms, leading in 8 out of the 11 sequences, with an average superiority of over 0.08 compared to ORB-SLAM3. It also outperformed other traditional algorithms by a large margin. Compared to other SLAM algorithms based deep learning, SL-SLAM also demonstrated significant advantages in terms of trajectory accuracy. Furthermore, due to the extraction and matching of more stable and distinctive feature points, resulting in more complete and accurate trajectories. The visualization of the trajectory as well as the ATE’s error is shown in Fig.7. It can be found that compared with the traditional geometric method ORB-SLAM3 of SOTA, the pose estimated by SL-SLAM is more stable and accurate.

At the same time, our method also supports monocular mode, we selected representative monocular slam algorithms for comparison, including DSO [17], SVO [31], DSM [32]. The Absolute Trajectory Error (ATE) of the estimated trajectories is shown in Table II. Among the 11 sequences in Euroc, SL-SLAM achieved SOTA results in 9 of them, with an average ATE surpassing ORB-SLAM3 by over 0.07. SL-SLAM significantly outperformed other algorithms. In sequence V203, where there is significant motion blur and photometric changes, ORB-SLAM3’s monocular mode failed to track successfully. However, due to SL-SLAM’s robust

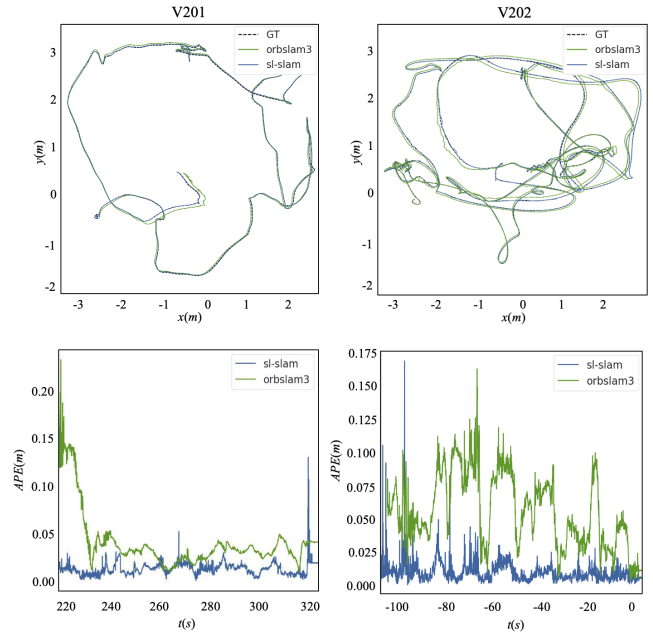


Fig. 7. Trajectory and Absolute Transition Error comparison of our SL-SLAM with ORBSLAM3 on the Euroc Dataset

feature extraction and matching methods, even with occasional tracking failures, it quickly relocalized, minimizing the impact of tracking failures. At the same time, due to the adoption of a more accurate closed-loop detection mechanism, multiple closed-loops are detected and corrected during operation, resulting in an ATE value of 0.031. In the meanwhile, our method also supports stereo and stereo-inertial sensor setups, experiments were conducted on the Euroc dataset. Table III shows the experimental results of ATE (RMSE) for stereo-inertial SL-SLAM on the Euroc dataset. We selected several representative stereo-inertial SLAM systems, including Vins-Fusion [33], BASALT [34], Kimera [35], and ORB-SLAM3 [15]. It can be observed that SL-SLAM achieved the best performance on 8 out of 11 sequences. Due to the leading effect of our method on multiple sensor Settings, it is enough to demonstrate the robustness as well as the high scalability of our method.

To further demonstrate the advantages of SL-SLAM comprehensively, we conducted experiments on the Tum-VI

TABLE II
RMSE[M] OF ATE COMPARISON WITH STATE-OF-THE-ART MONOCULAR METHODS ON EUROC. × MEANS IT FAILS IN THIS SEQUENCE. THE BEST RESULT IS HIGHLIGHTED IN BOLD

Dataset	DSO	SVO	DSM	ORB-SLAM3	Ours
MH01	0.046	0.100	0.039	0.016	0.007
MH02	0.046	0.120	0.036	0.027	0.032
MH03	0.172	0.410	0.055	0.028	0.022
MH04	3.810	0.430	0.057	0.138	0.014
MH05	0.110	0.300	0.067	0.072	0.038
V101	0.089	0.070	0.095	0.033	0.021
V102	0.107	0.210	0.059	0.015	0.015
V103	0.903	×	0.076	0.033	0.037
V201	0.044	0.110	0.056	0.023	0.021
V202	0.132	0.110	0.057	0.029	0.016
V203	1.152	1.080	0.784	×	0.031

TABLE III
RMSE[M] OF ATE COMPARISON WITH STATE-OF-THE-ART STEREO-VI METHODS ON EUROC. × MEANS IT FAILS IN THIS SEQUENCE. THE BEST RESULT IS HIGHLIGHTED IN BOLD

Dataset	VINS-Fusion	BASALT	Kimera	ORB-SLAM3	Ours
MH01	0.166	0.080	0.080	0.036	0.024
MH02	0.152	0.060	0.090	0.033	0.023
MH03	0.125	0.050	0.110	0.035	0.019
MH04	0.280	0.100	0.150	0.051	0.047
MH05	0.284	0.080	0.240	0.082	0.051
V101	0.076	0.040	0.050	0.038	0.033
V102	0.069	0.020	0.110	0.014	0.018
V103	0.114	0.030	0.120	0.024	0.022
V201	0.066	0.030	0.070	0.032	0.046
V202	0.091	0.020	0.100	0.014	0.012
V203	0.096	×	0.190	0.024	0.032

dataset. This dataset was captured by handheld devices and evaluated using visual-inertial odometry. Only the beginning and ending parts of the trajectory contain ground truth pose labels, which represent a small portion of the entire trajectory. Therefore, we followed the approach of ORB-SLAM3 to evaluate the accumulated drift of the entire trajectory. The results for monocular-inertial SL-SLAM are shown in the table IV. It can be observed that even for sequences with long trajectories, SL-SLAM achieves the lowest accumulated drift in most sequences, demonstrating the stability of our method.

C. Tracking robustness Evaluation

To verify the robustness of our method, we collected a dataset using our own equipment to simulate various challeng-

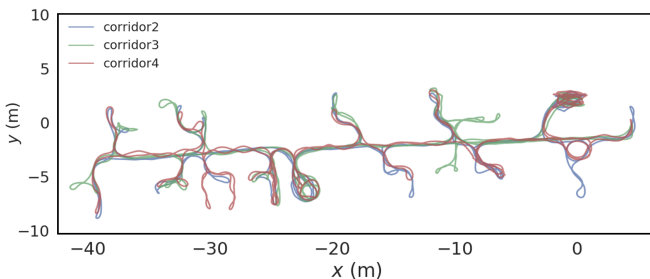


Fig. 8. Trajectory Visualization of SL-SLAM on the TUM-VI Dataset

TABLE IV
RMSE[M] OF ATE WITH SOTA VINS METHODS ON TUM-VI DATASET. THE BEST RESULT IS HIGHLIGHTED IN BOLD

Dataset	VINS-Mono	ORB-SLAM3	IMPS	Ours	length
corridor1	0.063	0.23	0.19	0.086	305
corridor2	0.095	0.04	0.04	0.062	322
corridor3	1.56	0.40	0.35	0.039	300
corridor4	0.25	0.16	0.15	0.007	114
corridor5	0.77	0.31	0.31	0.009	270
magistrale1	2.19	0.20	0.24	0.18	918
magistrale2	3.11	0.46	0.27	0.23	561

TABLE V
THE AVERAGE RUNNING TIME COMPARISON OF PRINCIPAL COMPONENTS WITH ORB-SLAM3 .

method	FE	TT	LM	PR	LC	ATE
ORB-SLAM3	11.98	23.22	191.50	3.45	124.77	0.058
Ours	7.27	27.41	223.89	0.37	110.71	0.023

ing environments and tested our method accordingly. We intentionally designed scenarios including changes in illumination, low-light conditions, low-texture environments, and severe camera motion. The handheld device used for data collection consists of a monocular camera (HIKVISION) with an image resolution of 1440×1080 , an IMU (Xsense) with a frequency of 100Hz, and an RTK module. Ground truth trajectories were obtained indoors using the Vicron motion capture system. Each frame of the image and IMU data were stored in rosbag format. Additionally, Gaussian white noise was added to the IMU data to simulate sensor faults. Under these conditions, as shown in the Fig.9, our method can clearly extract and track map points in low-texture areas and dark regions. Even with significant changes in illumination, the tracked map points remain relatively stable. In contrast, ORB-SLAM3 tends to lose track of map points and exhibits increasing drift, or even loses tracking altogether under such conditions. The quantitative analysis of the experimental results of orbslam3 and sl-slam is shown in Fig.10. Experimental results demonstrate that our method exhibits good robustness in these challenging environments, showing strong adaptability and stability.

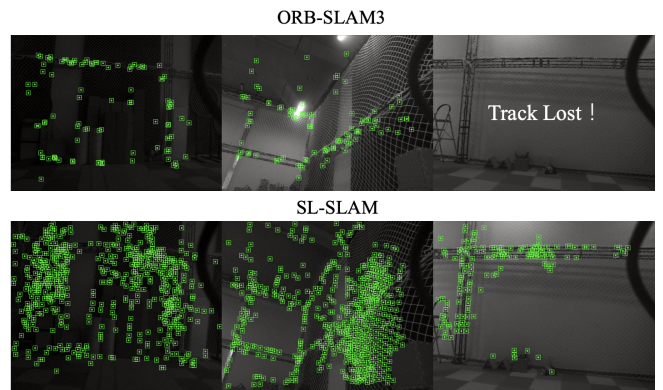


Fig. 9. Tracking Performance Comparison of SL-SLAM and ORB-SLAM3 on Our Dataset

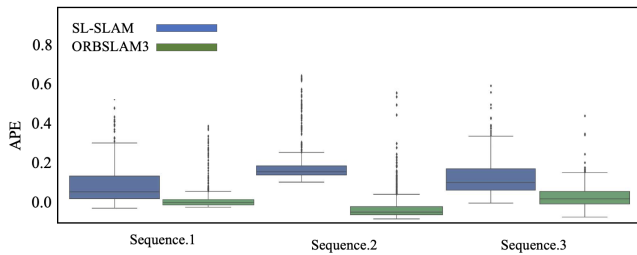


Fig. 10. The Absolute Transition Error Comparison of our SL-SLAM with ORBSLAM3 in our Datasets

TABLE VI
ABLATION STUDY. ABSOLUTE TRAJECTORY ERROR(RMSE AND STD) AND RELATIVE POSE ERROR(RMSE AND STD) ON EUROC V201 SEQUENCE

method	ATE(RMSE)	ATE(std)	RPE(RMSE)	RPE(std)
ours	0.0249	0.006	0.0047	0.0031
MT	0.0357	0.0156	0.0113	0.0102
LM	0.0391	0.0247	0.0195	0.0133
LC	0.0372	0.0205	0.0171	0.0142

D. Running Time Evaluation

To visually demonstrate the performance of the SLAM system, we conducted performance evaluations on its different modules to understand the impact of each module on the overall system runtime. The results are shown in table V, where FE represents the time for superpoint feature extraction, TT denotes the overall time for tracking each frame of the image, LM indicates the overall time for local mapping of a keyframe, and PR represents the time used for detecting similar frames using bag-of-words and performing geometric consistency checks. LC stands for the time taken for loop closure detection and overall trajectory correction. It can be observed that, due to the deployment of deep learning models using the ONNX Runtime framework, the feature extraction time is even shorter than that of ORB-SLAM3 when using GPU. Moreover, the time for tracking a single image frame is only slightly higher than that of ORB-SLAM3. As the feature matching quality is good and more matched feature points are triangulated, the time for local mapping is higher than that of ORB-SLAM3. Additionally, due to the better matching quality, we can recover sim3 transformations with fewer co-visible frames, and the overall loop closure correction time is also lower than that of ORB-SLAM3. Therefore, this system demonstrates good efficiency and is capable of real-time image tracking. It is important to note that since these modules run in parallel, the overall system runtime is not simply the sum of each module’s runtime.

E. Ablation Study

We conducted a series of experiments to systematically evaluate the efficacy of the modules proposed in our study. Initially, we integrated the tracking module from the baseline algorithm, incorporating both feature matching based on projection in a constant velocity motion model and bag-of-words feature matching in relocalization. This setup was denoted as

MT. Subsequently, we introduced the original triangulation-based mapping algorithm within the local mapping module, labeled as LM. For the loop closure detection module, we maintained the original feature matching algorithm while disabling the adaptive bundle adjustment, denoted as LC.

The results of these experiments, conducted on the Euroc dataset’s V201 sequence, are summarized in the accompanying table VI. Notably, we observed varying degrees of increase in ATE and RTE errors across the MT, LM, and LC algorithms compared to our model. Specifically, the ATE (RMSE) in MT, LM, and LC algorithms increased by 43%, 57%, and 49%, respectively. These findings underscore the importance of the proposed modules in enhancing the system’s overall performance.

In conclusion, our experiments demonstrate that integrating deep feature matching algorithms into different modules of the SLAM system contributes significantly to trajectory prediction accuracy. Furthermore, incorporating these modules throughout the entire SLAM process yields notable improvements in algorithmic performance.

V. CONCLUSION

In this paper, we proposed SL-SLAM, a versatile visual-inertial SLAM system that integrates deep learning-based feature point extraction and matching algorithms to achieve robust performance in challenging environments. Our approach leverages the SuperPoint feature extraction method and Lightglue matching algorithm, which have shown superior performance compared to traditional methods in terms of accuracy and robustness.

We use superpoint feature points throughout the whole process of the SLAM system, and adaptively adjust the number of adjustment points according to the complexity of the scene. At the same time, we build tracking, relocation, triangulation, loop closure detection methods based on lightglue, so that the method can adapt to the whole geometry-based SLAM framework in the deep feature and matching method. Through qualitative and quantitative analysis of the state-of-the-arts method with various sensor types on the public data set and self-collected data set, the effectiveness and robustness of SL-SLAM in a variety of challenging environments are demonstrated. In the future, we will explore how to use deep feature extraction and matching to achieve simultaneous localization and mapping of multi-agents.

REFERENCES

- [1] S. Wen, Y. Zhao, X. Yuan, Z. Wang, D. Zhang, and L. Manfredi, “Path planning for active slam based on deep reinforcement learning under unknown environments,” *Intelligent Service Robotics*, vol. 13, pp. 263–272, 2020.
- [2] J. Cheng, L. Zhang, Q. Chen, X. Hu, and J. Cai, “A review of visual slam methods for autonomous driving vehicles,” *Engineering Applications of Artificial Intelligence*, vol. 114, p. 104992, 2022.
- [3] Y. Zhao, L. Chen, X. Zhang, S. Xu, S. Bu, H. Jiang, P. Han, K. Li, and G. Wan, “Rtsfm: Real-time structure from motion for mosaicing and dsm mapping of sequential aerial images with low overlap,” *IEEE Transactions on Geoscience and Remote Sensing*, vol. 60, pp. 1–15, 2021.
- [4] A. Macario Barros, M. Michel, Y. Moline, G. Corre, and F. Carrel, “A comprehensive survey of visual slam algorithms,” *Robotics*, vol. 11, no. 1, p. 24, 2022.

- [5] R. Mur-Artal and J. D. Tardós, “Orb-slam2: An open-source slam system for monocular, stereo, and rgb-d cameras,” *IEEE transactions on robotics*, vol. 33, no. 5, pp. 1255–1262, 2017.
- [6] T. Qin, P. Li, and S. Shen, “Vins-mono: A robust and versatile monocular visual-inertial state estimator,” *IEEE Transactions on Robotics*, vol. 34, no. 4, pp. 1004–1020, 2018.
- [7] C. Kerl, J. Sturm, and D. Cremers, “Dense visual slam for rgb-d cameras,” in *2013 IEEE/RSJ International Conference on Intelligent Robots and Systems*. IEEE, 2013, pp. 2100–2106.
- [8] A. I. Mourikis and S. I. Roumeliotis, “A multi-state constraint kalman filter for vision-aided inertial navigation,” in *Proceedings 2007 IEEE international conference on robotics and automation*. IEEE, 2007, pp. 3565–3572.
- [9] Z. Teed and J. Deng, “Droid-slam: Deep visual slam for monocular, stereo, and rgb-d cameras,” *Advances in neural information processing systems*, vol. 34, pp. 16 558–16 569, 2021.
- [10] Z. Zhu, S. Peng, V. Larsson, W. Xu, H. Bao, Z. Cui, M. R. Oswald, and M. Pollefeys, “Nice-slam: Neural implicit scalable encoding for slam,” in *Proceedings of the IEEE/CVF Conference on Computer Vision and Pattern Recognition*, 2022, pp. 12 786–12 796.
- [11] X. Peng, Z. Liu, W. Li, P. Tan, S. Cho, and Q. Wang, “Dvi-slam: A dual visual inertial slam network,” *arXiv preprint arXiv:2309.13814*, 2023.
- [12] D. Li, X. Shi, Q. Long, S. Liu, W. Yang, F. Wang, Q. Wei, and F. Qiao, “Dxslam: A robust and efficient visual slam system with deep features,” in *2020 IEEE/RSJ International conference on intelligent robots and systems (IROS)*. IEEE, 2020, pp. 4958–4965.
- [13] Y. Wang, B. Xu, W. Fan, and C. Xiang, “A robust and efficient loop closure detection approach for hybrid ground/aerial vehicles,” *Drones*, p. 135, Feb 2023. [Online]. Available: <http://dx.doi.org/10.3390/drones7020135>
- [14] P. Lindenberger, P.-E. Sarlin, and M. Pollefeys, “Lightglue: Local feature matching at light speed,” in *Proceedings of the IEEE/CVF International Conference on Computer Vision*, 2023, pp. 17 627–17 638.
- [15] C. Campos, R. Elvira, J. J. G. Rodríguez, J. M. Montiel, and J. D. Tardós, “Orb-slam3: An accurate open-source library for visual, visual-inertial, and multimap slam,” *IEEE Transactions on Robotics*, vol. 37, no. 6, pp. 1874–1890, 2021.
- [16] S. Sumikura, M. Shibuya, and K. Sakurada, “Openvslam: A versatile visual slam framework,” in *Proceedings of the 27th ACM International Conference on Multimedia*, 2019, pp. 2292–2295.
- [17] J. Engel, V. Koltun, and D. Cremers, “Direct sparse odometry,” *IEEE transactions on pattern analysis and machine intelligence*, vol. 40, no. 3, pp. 611–625, 2017.
- [18] R. Li, S. Wang, Z. Long, and D. Gu, “Undeepvo: Monocular visual odometry through unsupervised deep learning,” in *2018 IEEE international conference on robotics and automation (ICRA)*. IEEE, 2018, pp. 7286–7291.
- [19] N. Yang, L. v. Stumberg, R. Wang, and D. Cremers, “D3vo: Deep depth, deep pose and deep uncertainty for monocular visual odometry,” in *Proceedings of the IEEE/CVF conference on computer vision and pattern recognition*, 2020, pp. 1281–1292.
- [20] Z. Teed, L. Lipson, and J. Deng, “Deep patch visual odometry,” *Advances in Neural Information Processing Systems*, vol. 36, 2024.
- [21] H. M. S. Bruno and E. L. Colombari, “Lift-slam: A deep-learning feature-based monocular visual slam method,” *Neurocomputing*, vol. 455, pp. 97–110, 2021.
- [22] J. Tang, L. Ericson, J. Folkesson, and P. Jensfelt, “Gcnv2: Efficient correspondence prediction for real-time slam,” *IEEE Robotics and Automation Letters*, vol. 4, no. 4, pp. 3505–3512, 2019.
- [23] K. Xu, Y. Hao, S. Yuan, C. Wang, and L. Xie, “Airvo: An illumination-robust point-line visual odometry,” in *2023 IEEE/RSJ International Conference on Intelligent Robots and Systems (IROS)*. IEEE, 2023, pp. 3429–3436.
- [24] Y. Wang, B. Xu, W. Fan, and C. Xiang, “A robust and efficient loop closure detection approach for hybrid ground/aerial vehicles,” *Drones*, vol. 7, no. 2, p. 135, 2023.
- [25] M. Burri, J. Nikolic, P. Gohl, T. Schneider, J. Rehder, S. Omari, M. W. Achtelik, and R. Siegwart, “The euroc micro aerial vehicle datasets,” *The International Journal of Robotics Research*, vol. 35, no. 10, pp. 1157–1163, 2016.
- [26] D. Schubert, T. Goll, N. Demmel, V. Usenko, J. Stückler, and D. Cremers, “The tum vi benchmark for evaluating visual-inertial odometry,” in *2018 IEEE/RSJ International Conference on Intelligent Robots and Systems (IROS)*. IEEE, 2018, pp. 1680–1687.
- [27] L. Von Stumberg, V. Usenko, and D. Cremers, “Direct sparse visual-inertial odometry using dynamic marginalization,” in *2018 IEEE International Conference on Robotics and Automation (ICRA)*. IEEE, 2018, pp. 2510–2517.
- [28] R. Mur-Artal and J. D. Tardós, “Visual-inertial monocular slam with map reuse,” *IEEE Robotics and Automation Letters*, vol. 2, no. 2, pp. 796–803, 2017.
- [29] S. Leutenegger, P. Furgale, V. Rabaud, M. Chli, K. Konolige, and R. Siegwart, “Keyframe-based visual-inertial slam using nonlinear optimization,” *Proceedings of Robotis Science and Systems (RSS) 2013*, 2013.
- [30] X. Peng, Z. Liu, W. Li, P. Tan, S. Cho, and Q. Wang, “Dvi-slam: A dual visual inertial slam network,” *arXiv preprint arXiv:2309.13814*, 2023.
- [31] C. Forster, M. Pizzoli, and D. Scaramuzza, “Svo: Fast semi-direct monocular visual odometry,” in *2014 IEEE international conference on robotics and automation (ICRA)*. IEEE, 2014, pp. 15–22.
- [32] J. Zubizarreta, I. Aguinaga, and J. M. M. Montiel, “Direct sparse mapping,” *IEEE Transactions on Robotics*, vol. 36, no. 4, pp. 1363–1370, 2020.
- [33] T. Qin, J. Pan, S. Cao, and S. Shen, “A general optimization-based framework for local odometry estimation with multiple sensors,” *arXiv preprint arXiv:1901.03638*, 2019.
- [34] V. Usenko, N. Demmel, D. Schubert, J. Stückler, and D. Cremers, “Visual-inertial mapping with non-linear factor recovery,” *IEEE Robotics and Automation Letters*, vol. 5, no. 2, pp. 422–429, 2019.
- [35] Y. Tian, Y. Chang, F. H. Arias, C. Nieto-Granda, J. P. How, and L. Carlone, “Kimera-multi: Robust, distributed, dense metric-semantic slam for multi-robot systems,” *IEEE Transactions on Robotics*, vol. 38, no. 4, 2022.